Influence of Anion Adsorption on the Step Dynamics on Au (111) Electrodes

Margret Giesen[1 *] and Dieter M. Kolb[2]

[1] Institut für Grenzflächenforschung und Vakuumphysik, Forschungszentrum Jülich, 52425 Jülich, Germany

[2] Abteilung Elektrochemie, Universität Ulm, 89069 Ulm, Germany

Using scanning tunneling microscopy, we have investigated the step dynamics on a Au(111) single crystal electrode in aqueous electrolytes. Our studies focused on the influence of specifically adsorbed anions as well as of the anion concentration on the mobility of gold atoms at monatomic high step edges. The experiments were performed in chloride-containing and chloride-free H_2SO_4-electrolytes. From the quantitative analysis of equilibrium step fluctuations we deduce the dominant mass transport mechanisms as a function of the electrode potential and as a function of the anion concentration. Estimates of the energies involved in the mass transport are presented.

* Corresponding author; Electronic mail: m.giesen@fz-juelich.de

1. Introduction

In many reactions at the solid/liquid interface defects like steps play a significant role. Steps are preferred adsorption sites with an enhanced binding energy for the adsorbed species on the one hand. On the other hand, detachment of atoms also begins at steps due to the reduced binding energy compared to that for atoms within a close-packed layer. In order to fully understand the dynamics of reactions at electrode surfaces it is important to study the basic atomic processes involved. While investigations of the atomic diffusion on solid surfaces in ultra high vacuum (UHV) are frequently performed, studies of the atomic motion on surfaces in an electrochemical environment have been scarce [1, 2]. Meanwhile, however, several groups employ scanning probe techniques like scanning tunneling microscopy (STM) [3] to the investigation of atomic diffusion at the electrochemical interface. Examples of studies of the dynamics at the solid/liquid interface are the investigation of the potential induced lifting of the reconstruction on Au(100) electrodes [4], the dynamics of Ag(111) surfaces [5] or the formation of ordered adlayers and their influence on the step structure on Cu(100) and (111) electrodes [6, 7]. Despite these efforts, quantitative information about diffusion rates, activation barriers for diffusion along or across steps and other energetic parameters which contribute to the dynamics on surfaces are still lacking. First attempts in this direction were made recently by the analysis of the equilibrium fluctuations of monatomic high steps on Ag (111) and Cu (100) interfaces [8-10]. The analysis of the time dependence of step fluctuations is a frequently applied and common method to study mass transport on surfaces in UHV on the atomic scale. There, metal surfaces as well as semiconductor surfaces have been investigated [11-20]. The analysis of equilibrium step fluctuations permits the determination of the dominant mass transport processes [20-23]. With the help of

temperature dependent studies, the corresponding activation barriers can be measured.

The theoretical and experimental tools developed for UHV investigations can be applied in principle also to surfaces in an electrochemical environment. However, in contrast to UHV where the vapor phase can be neglected, the electrolyte takes part in the solid/liquid interface and therefore has a significant influence on the interface dynamics. While temperature dependent studies in an electrochemical cell are more difficult to perform than in UHV, it has been demonstrated that activation energies can be estimated by measuring step fluctuations at room temperature for various electrode potentials [8, 9].

Here, we present a detailed study of step fluctuations on Au(111) electrodes as a function of electrode potential and for the case of a specifically adsorbed anion. As an electrolyte, we have used 0.1M sulfuric acid with and without different concentrations of HCl added. We determined the dominant atomic processes for the step fluctuations and give rough estimates for the relevant energies involved.

2. Experimental

The experiments were performed with the electrochemical version of the Topometrix Discoverer TMX 2010 scanning tunneling microscope (STM), which permits an independent control of the sample and the tip potential by a bipotentiostat. The STM tips were etched from a 0.25 mm diameter polycrystalline tungsten wire and coated with an electrophoretic paint [24] to reduce the area in contact with the electrolyte down to 10^{-7}-10^{-8} cm^2 [25]. The tunneling current was 2 nA in all experiments. It was shown previously that tunneling currents of the order of 1-3 nA have no influence on the measurements of the step mobility on Ag(111) electrodes in aqueous electrolyte (at least for not too positive electrode potentials) [9]. Since the adatom mobility on Ag (111) is higher than that on a Au(111) surface and the potential range studied is well

below the onset of oxidation of Au(111), it is reasonable to assume that the influence of the tip on our measurements is negligible. All images were obtained in the constant-current mode. They are unfiltered, but corrected for any tilt of the sample, where necessary.

The experiments were performed in 0.1 M H_2SO_4 with (A) no, (B) 0.01 mM, (C) 0.5 mM, (D) 1 mM, (E) 5 mM and (F) 50 mM HCl added. The electrolytes were made from suprapure chemicals (Merck) and Milli-Q water (Millipore) with a specific resistance of 18.2 MΩcm and 3 ppb TOC. In the experiments, two Pt wires served as reference and counter electrodes. However, all potentials are quoted with respect to the saturated calomel electrode (SCE).

The Au(111) crystal was a disc of 12 mm diameter and 2 mm thickness and commercially supplied by MaTecK (Jülich). It had a small miscut about the $[11\bar{2}]$-direction such that the crystal surface revealed parallel, (111)-oriented steps (B-steps) which we checked by atomically resolved STM images of steps and the adjacent terraces. Before mounting the crystal in the electrochemical cell, the crystal was flame-annealed in a hydrogen flame for 4-6 min at yellow heat and cooled in a flux of nitrogen. After preparation, the crystal was mounted in the electrochemical STM cell and the electrolyte added under potential control. We used an initial potential of U_S = –200mV vs. SCE for the electrolytes with a HCl - concentration up to 0.5 mM. For higher HCl - concentrations, contact with the electrolyte was established at $U_S = -100$ or -50mV vs. SCE to avoid evolution of hydrogen. At these potentials, the Au(111) surface is known to be reconstructed [4]. The measurements were started only, when the reconstruction of the Au(111) surface was clearly visible in the beginning. Due to the specific adsorption of anions at more positive potentials, the reconstruction is lifted. For the electrolytes (A), (B) and (C), the reconstruction started to lift around + 250mV vs. SCE. Due to the higher anion

concentration in the electrolytes (D) to (F), the lifting of the reconstruction began between + 50mV and – 50mV vs. SCE [4, 26].

After the first contact with the electrolyte, the surface revealed large reconstructed terraces (up to 5 µm width) and parallel steps along $\langle 01\bar{1} \rangle$. Occasionally, pinning centers by residual contamination and dislocations were observed. The mean distance between these defects, however, was of the order of several µm. For the analysis we chose merely B-steps along the densely-packed $\langle 01\bar{1} \rangle$ directions with no obvious contamination present. These steps are free of forced kinks which influence the measurements.

In addition to the STM experiments, we performed cyclic voltammetry in normal electrochemical cells with cylindrically shaped, nominally (111)-oriented Au-crystals of about 4 mm height and 0,125 cm² surface area (also commercially supplied by MaTecK (Jülich)). The crystals were flame-annealed for approximately 4 min with a Bunsen burner and allowed to cool in air for 75 s. Then, the (111) surface was covered with a drop of Millipore water before mounting the crystal in the electrochemical cell. The electrolyte was purged with a high flux of nitrogen gas to remove the oxygen. After 10-20 min, the crystal was brought into contact with the electrolyte under potential control. Prior to the measurement, the electrolyte was purged for another 30-40 min until the leak current was below 100 nA. In all experiments, the immersion potential was - 250mV vs. SCE. The potential scan was started in positive direction up to +800 or +850mV vs. SCE before the scan direction was reversed. The scan rate was always 10 mV/s.

3. Theory and results

Fig. 1 shows STM images of a stepped area of the Au(111) surface at room temperature for different electrode potentials (a) 0 mV and (b) + 400mV vs. SCE in

0.1M H_2SO_4 containing 5mM HCl. The scan width in both images is 150 nm. The images are not normal STM images, but so-called time images [27]. In time images, a single line is scanned repetitively and displayed in the normal STM image format. Hence, one axis is a time rather than a spatial axis. In our experiments, the spatial axis is always (almost) perpendicular to the mean step orientation and the time axis is parallel to the step edges. The "step edges" in the STM images shown here, however, represent not real step edges but the time evolution of a distinct step position in a single scan line.

The step edges shown in Fig. 1 are not straight but reveal a certain kind of roughness that was denoted as "frizziness" [28-30]. The frizziness of steps arises from rapid kink motion along steps. Whenever a kink crosses a scan line, a sudden shift in the step position is observed. The frizziness of steps was first explained properly by Wolf et al. for steps on a Ag(111) surface under UHV conditions [28]. Later, Dietterle et al. investigated the same phenomenon for steps on a Ag(111) electrode in an aqueous electrolyte [5]. Meanwhile, the frizziness of steps has been observed and studied on many metal systems in UHV [11-20, 30, 31] as well as in electrochemical environment [8-10, 32-34].

The frizziness of steps is a measure of the equilibrium fluctuations of steps due to the motion of atoms and kink sites. Equilibrium fluctuations may be quantitatively analyzed by means of a step correlation function F(t):

$$F(t) = \left\langle (x(t) - x(0))^2 \right\rangle \qquad (1)$$

Here, x denotes the coordinate along the spatial axis perpendicular to the steps and t is the time. As in eq.(1), the reference time may be set to zero. To compensate for

thermal drift of the STM (as becomes obvious from the non-vertical orientation of the step edges in Fig. 1) it is convenient to analyze a step pair correlation function where Δx is the difference in step positions of neighboring steps in the same scan line:

$$F(t) = \frac{1}{2}\left\langle \left(\Delta x(t) - \Delta x(0)\right)^2 \right\rangle \qquad (2)$$

Depending on the mass transport involved in the fluctuations, the time correlation function F(t) obeys different time laws. Theoretical overviews are given in refs. [21-23] and an overview adapted to the needs of an experimentalist in ref. [8]. Here, we will summarize only the theoretical equations needed for our purposes. The basic result is that the time correlation function obeys a power law of the form

$$F(t) = c_{\alpha,\delta}(T)\, L^{\delta}\, t^{\alpha} \qquad (3)$$

Here, L denotes the mean distance between the steps and $c_{\alpha,\delta}(T)$ is a temperature dependent pre-factor which is different for the different exponents δ and α and contains all energy-related quantities. The exponents δ and α depend on the mass transport mechanism dominating the step fluctuations.

When the atomic motion is restricted to the step edges, F(t) is given by [14, 35]

$$F(t) = P_k^{3/4} \left(a_{\perp}^2\, a_{||}^3\, c_{st}\, D_{st}\right)^{1/4}\, t^{1/4} \qquad (4)$$

The nearest-neighbor distance $a_{||}$ is measured along $\langle 110 \rangle$ and $a_{\perp}$ is the distance between atomic rows ($a_{||}$=2.89 Å and $a_{\perp}$ = 2.50 Å for Au(111)). The kink concentration P_k can be expressed in terms of the kink formation energy ε [29, 36]:

$$P_k = \frac{2a_{\perp}^2/a_{||}}{e^{\varepsilon/k_BT} + e^{-\varepsilon/k_BT} - 2} \approx 2\frac{a_{\perp}^2}{a_{||}} e^{-\varepsilon/k_BT} \quad (\varepsilon >> k_BT) \qquad (5)$$

The second term in eq. (5) holds for not too large temperatures. In eq. (4), c_{st} and D_{st} are the adatom concentration at steps and the diffusion constant for atomic motion along steps, respectively. In the case of motion along steps, the exponents δ and α (eq. (3)) are 0 and 1/4, respectively. The time exponent α is also 1/4 for the case that mass is exchanged with neighboring terraces but atoms are reflected at the neighboring step edges due to the presence of an Ehrlich-Schwoebel barrier [37, 38]. Then, however, the exponent δ is 1/4 rather than 0 [21-23].

A time exponent α = 1/2 is observed when mass is exchanged between steps and terraces and the diffusion on the terrace is fast compared to the attachment/detachment of atoms at steps. In addition, the mean diffusion length of the atoms perpendicular to the steps is supposed to be much smaller than the mean step-step distance. Then, F(t) is

$$F(t) = P_k^{1/2} \left(\frac{a_{\perp}^2 a_{||}}{\tau_a} \right)^{1/2} t^{1/2} \qquad (6)$$

τ_a is the mean time between evaporation processes of adatoms from kink sites onto the terrace. Here, the exponents δ and α (eq. (3)) are 0 and 1/2, respectively. F(t) is

proportional to $t^{1/2}$ also for two further mass transport situations. One is, when atoms are exchanged with the terrace as well as with the adjacent phase which in our case would be the electrolyte. In this case, the time correlation function depends on the mean step-step distance as $L^{+1/2}$. In the second $t^{1/2}$ - case, atoms are exchanged with the neighboring terraces and atoms are allowed to cross neighboring steps. Then, F(t) is proportional to $L^{-1/2}$ [21-23].

Using normal STM images rather than time images, one may also analyse the spatial correlation function F(y)

$$F(y) = \left\langle \left(x(y) - x(0)\right)^2 \right\rangle = P_k\, y \qquad (7)$$

where x is again the coordinate perpendicular to the steps and y is now the spatial axis along the steps in units of $a_\perp$ and $a_{||}$, respectively. F(y) is linear in y and the factor is the kink concentration P_k [29, 36]. By measuring F(y) from normal STM images, one obtains a value for the kink formation energy ε per atom.

3.1 The time dependence of F(t)

In our experiments, we have analyzed the time correlation function for different electrode potentials and different electrolytes and determined the exponents α and δ. First, we present the experimental results for the chloride containing electrolytes.

(a) Au(111) in 0.1 M H_2SO_4 + x mM HCl

Fig. 2 shows the time correlation function (open circles) for the Au(111) surface in 0.1M H_2SO_4 containing 1mM HCl for electrode potentials (a) + 200 mV and (b) + 600mV vs. SCE. The solid line in Fig. 2(a) is a least square fit to the experimental data of the form

$$F(t) = \text{const. } t^{1/2} \qquad (8)$$

In contrast to what is observed for Ag(111) in solution [8], no finite intersection with the y-axis is needed to fit the data for Au(111)[1]. In Fig. 2(a), the dashed curve shows the best fit to the data using a time exponent 1/4 rather than 1/2 in eq. (8). Obviously, the experimental result is not in agreement with a time exponent 1/4.

The experimental data at U_S = + 600 mV, on the other hand, are best fitted by a time correlation function (solid line)

$$F(t) = \text{const. } t^{1/4}, \qquad (9)$$

whereas a fit with a time exponent 1/2 yields no satisfying agreement with the data (dashed line in Fig. 2(b)). We have analyzed the time exponents for electrode potentials between $U_S = -200\text{mV}$ and $+ 650\text{mV}$ vs. SCE for HCl concentrations between 0.01 and 50mM. We find that below U_S = + 300mV, the time exponent is 1/2. For potentials above U_S = + 300mV, the experimental data are best fitted by a time exponent 1/4. We note, that the time exponent measured in a potential range of about 100mV around + 300mV vs. SCE changes gradually from 1/2 to 1/4 rather than by a sudden transition, i.e., starting from negative potentials and small positive potentials (where α is 1/2), the time exponent increases and assumes values close

[1] A constant off-set F(0)≠0 was, however, observed for Au(111) in KI and $KClO_4$ by McHardy et al. [34]: These authors found that F(t) is non-zero for t=0 in the potential range where iodine is adsorbed on the surface in a disordered phase. The physical origin of the offset at t=0 as well as the question as to why F(t) has a constant contribution for Au(111) in KI and $KClO_4$ but not in H_2SO_4 and HCl is not understood yet. It was proposed that F(0) may be due to tip-surface interactions [8] which, however, was not confirmed by studies of the time correlation function for various tunneling conditions [9]. Hence, a detailed understanding is still lacking. One may note, however, that the existence of a constant contribution at F(t=0) requires particular care when analyzing the time dependence of F(t).

to 1/3 (higher than +250 and lower than +350 mV) until it reaches the value of 1/4 at potentials larger than +350mV vs. SCE. It is emphasized, however, that the measured time exponent close to 1/3 in the transition regime is not related to a further dominant mass transport mechanism (terrace exchange with slow terrace diffusion [20-23]), but is rather due to the onset of edge diffusion and a significant contribution of edge diffusion to F(t) in the transition range.

In order to identify the dominant mass transport mechanism in the two potential regimes, one has to measure the dependence of F(t) on the mean step-step distance L. Fig. 3 shows log-log plots of the time correlation function at t=1s vs. the step-step distance L for 0.1M H_2SO_4 containing 0.5mM HCl. The open circles represent the experimental data for (a) + 250mV and (b) + 600mV vs. SCE. The straight lines correspond to the theoretical solutions for the different exponents δ (eq. (3)) as denoted in the figure. The theoretical solutions are not scaled with respect to the absolute value of F(1s). Hence, we would like to draw the reader's attention exclusively to the slopes of the straight lines. Despite the scattering of the experimental data, agreement with the theoretical solution is achieved only for δ=0 in both potential ranges. That is, regardless of the electrode potential, the time correlation function does not depend on the mean distance between adjacent steps. Hence, for potentials below + 300mV vs. SCE the dominant mass transport mechanism is fast terrace diffusion (eq.(6))[2]. For potentials above + 300mV vs. SCE, the mass transport is predominantly restricted to the step edges (eq. (4)). The same result is found for all electrolytes independent of the chloride concentration.

(b) Au(111) in chloride-free 0.1 M H_2SO_4

[2] Note that the independence of F(t) on the step-step distance L automatically indicates that no significant amount of Au atoms is exchanged between the surface and the electrolyte, i.e., dissolution of Au is negligible.

We have studied the time correlation function for the chloride-free electrolyte (A) in a potential range between − 200 and + 830mV vs. SCE. These studies were more difficult than those in the HCl-containing electrolytes. The determination of the time exponent of F(t) as a function of the electrode potential was very sensitive to pinning of the steps by Au islands which were on the surface after lifting the reconstruction. (Such islands are readily removed in chloride-containing solutions by the so-called electrochemical annealing [39, 40].) On the other hand, in the cathodic potential range where the surface is reconstructed, the diffusivity is so low that even time images display primarily spatial information due to the remaining thermal drift of the surface. Therefore, we were not able to achieve a reliable statistical data base for the time exponents.

3.2 The potential dependence of F(t) for constant time

We have studied the step fluctuations as a function of the electrode potential for constant time. In Fig. 4 the value of the time correlation function at t=1s, F(1s), is plotted vs. the electrode potential for five different chloride concentrations (as indicated in the figure). For all chloride concentrations an increase of the step fluctuations with increasing electrode potential is observed. The data are well fitted by an exponential dependence (solid and dotted curves). A strong increase of the step fluctuations is observed around + 300mV vs. SCE for the electrolytes (C)-(F), i.e., for chloride concentrations between 0.5mM and 50mM. While the data does not allow to distinguish small shifts in the potential of ±50mV, the potential where the fluctuations increase corresponds approximately to the potential of zero charge (pzc) of Au(111) (about + 300mV [26, 41, 42]). Whereas the data for higher Cl^- concentrations lie on one and the same exponential curve, the data measured in electrolyte (F) (containing 0.01mM HCl) are clearly lower.

Though reliable information on the time dependence of F(t) was obtained only for the chloride containing electrolytes, we were able to study the potential dependence of F(t) for all electrolytes (A) - (F) including chloride-free solution. It is well known that Cl^- is more strongly adsorbed than SO_4^{2-} [43, 44]. While sulfate is the only specifically adsorbed anion in the chloride-free electrolyte (A), the sulfate is gradually replaced by chloride for the electrolytes (B)-(F). Hence, by comparing the results obtained for the chloride-free electrolyte (A) and the chloride-containing electrolytes, the influence of the specifically adsorbed Cl^- on the step fluctuations may be studied. This is shown in Fig. 5 where F(1s) is plotted for three different cases. The circles correspond to the averaged data for the electrolytes (C)-(F) (0.5mM Cl^- and higher), the squares to the data for electrolyte (B), and the triangles to the data for the chloride-free electrolyte (A). For potentials below about + 100mV vs. SCE, there is no measurable difference between the data obtained in the various electrolytes. Around +300mV vs. SCE, however, the data for the electrolytes with Cl^- concentrations higher than 0.01 mM strongly deviate from those obtained for the chloride-free electrolyte (A). In the latter case, the step fluctuations remain much smaller - though they also slightly increase with potential.

In the chloride-free electrolyte (A), the $(\sqrt{3} \times \sqrt{7})$R19.1°-sulfate superstructure is formed for potentials around + 800mV vs. SCE [45]. After the formation of this superstructure, the step edges still appear frizzy. In Fig. 5, the results obtained for F(1s) at + 830mV vs. SCE are included and marked by an arrow. The two data points were obtained from independent measurements and fit into the general behavior of F(1s) for more negative potentials.

3.3 The kink formation energy in the cathodic potential range

For the chloride-containing electrolyte (C) (with 0.5mM HCl), we have determined the kink formation energy ε^{Cl^-} by the analysis of a spatial rather than a time correlation function [46]. Fig. 6 shows the spatial correlation function F(y) at $U_S = -100$mV vs. SCE. The experimental data (open circles) are fitted by a straight line. From the slope we determine the kink formation energy at $U_S = -100$mV vs. SCE (using eqs. (5)-(7)) to

$$\varepsilon^{Cl^-} = 0.074 \pm 0.002 \text{eV / atom} \qquad (10)$$

3.4 Voltammetric measurements

Fig. 7 shows cyclic voltammograms measured in 0.1M H_2SO_4 with (a) no HCl, (b) 0.01mM HCl and (c) 1mM HCl added. In the chloride-free case (a), the peak at + 326mV corresponds to the lifting of the surface reconstruction caused by non-ordered specifically adsorbed sulfate. The peaks at + 784 and + 760mV vs. SCE are related to the formation and the lifting of the $\left(\sqrt{3} \times \sqrt{7}\right)$-sulfate adlayer [45], respectively. Satellite peaks are visible at slightly more positive potentials (+ 800 and + 789mV vs. SCE). These satellite peaks have been attributed to additionally adsorbed sulfate [45], to co-adsorbed hydronium [47] and water [48]. When 0.01mM HCl is added to the electrolyte (solid curve), the lifting of the reconstruction is shifted to more negative potentials (+ 288mV vs. SCE), however, the peak related to the formation of the ordered sulfate layer is not affected. The corresponding peak for the lifting of the $\left(\sqrt{3} \times \sqrt{7}\right)$-sulfate adlayer is nevertheless much smaller.

A raising current is observed for electrode potentials higher than + 784mV. This increase is related to the slow formation of an ordered chloride $\left(\sqrt{3} \times \sqrt{3}\right)$R30° adlayer [49], as was shown in previous measurements [50]. This peak shifts to

691mV vs. SCE when 1mM HCl is added to the electrolyte [51]. Furthermore, no satellite peaks are observed for Au(111) in 0.1M H_2SO_4 + 0.01mM HCl. We will return to this point later.

4. Discussion

4.1 The potential dependence of the time exponent

Here, we restrict ourselves primarily to the discussion of the results obtained for the chloride-containing electrolytes. As shown in Figs. 2 and 3, there are two potential ranges where the step fluctuations obey different time laws independent of the chloride concentration. For electrode potentials far below + 300mV vs. SCE F(t) is proportional to $t^{1/2}$, above + 300mV to $t^{1/4}$. In both cases, F(t) is independent of the step-step distance L. According to [21-23], the dominant mass transport must therefore be restricted along the steps for U_S > + 300mV vs. SCE. In the potential range U_S < + 300 mV, mass is predominantly exchanged between steps and the adjacent lower terraces[3]. This result seems surprising at first glance: For metal surfaces under ultra high vacuum (UHV) conditions for instance, the diffusion barrier along steps is smaller than the activation barrier for detachment of atoms from kink sites onto the terrace [13, 52, 53]. Hence, at low temperatures step fluctuations are generally dominated by step edge diffusion while atom detachment from steps to the terrace becomes dominant at higher temperatures [13]. For metal electrodes in electrolyte the activation energies of the mass transport processes contributing to the step dynamics decrease with increasing electrode potential. In the case of metal dissolution, the desorption enthalpy vanishes. Therefore, it is a priori reasonable to assume that step fluctuations were dominated by edge diffusion at negative potentials and by atom detachment from steps to the terrace at positive potentials.

[3] Note that any other mass transport process as, e.g., exchange of atoms between neighboring steps and/or exchange between the electrode surface and the electrolyte would manifest itself in a dependence of F(t) on the step-step distance (see, e.g., case "D" of [21]).

However, the opposite seems to be the case for Au (111) in Cl^- containing electrolytes. We interpret our results such that the strong specific adsorption of chloride around the pzc [54] reduces the diffusion barrier along steps and/or the kink creation energy. The reduction of the energies may shift the energy balance from terrace diffusion to edge diffusion, and hence, lead to a transition in the dominant mass transport mechanism while the contribution of terrace diffusion to F(t) remains unaltered (at least for dilute chloride containing electrolytes where merely the steps are covered by chloride ions, as discussed below).

Since F(t) increases substantially upon chloride adsorption, we can, however, not exclude that the contribution of terrace diffusion to F(t) in fact decreases. The decrease may be due to the change of atom density in the surface layer when the surface reconstruction is lifted: In the reconstructed phase below +300mV vs. SCE, the density of surface atoms is 4% higher than in the unreconstructed phase above +300mV vs. SCE. STM studies of Ni adatom mobilities on Ru(0001) in UHV showed that the energy barrier for adatom diffusion on the surface decreases with increasing density of atoms in the surface layer [55]. For the case of Ag diffusion on Ag(111), calculations by Ratsch et al. [56] showed that the diffusion barrier increases with increasing lattice constant. A similar trend may be expected for Au adatom diffusion on Au(111) in electrolyte. In the dense reconstructed phase, the surface diffusion barrier may be smaller than in the less dense unreconstructed phase such that after lifting of the reconstruction the contribution of terrace diffusion to F(t) is further reduced compared to the contribution of edge diffusion.

4.2 Dependence of the step fluctuations on the electrolyte composition

Specific adsorption of anions such as chloride and sulfate on Au(111) dominates for electrode potentials larger than the potential of zero charge (pzc) which is approximately around + 300mV vs. SCE [26, 41]. The step fluctuations increase with

anions specifically adsorbed on the surface. In the case of sulfate adsorption the increase of the step fluctuations is only gradually whereas for chloride adsorption the fluctuations may increase up to a factor of 10 depending on the Cl^- concentration and the electrode potential (Figs. 4 and 5). It is rather striking that the influence of the chloride atoms adsorbed on the surface on the step fluctuations seems to be saturated already for a Cl^- concentration of 0.05mM (Fig. 4). For Cl^- concentrations between 0.1 and 50mM no measurable difference in the data is observed, and the data for electrolyte (B) (containing 0.01mM HCl) are only slightly below those for electrolytes (C)-(F). It is therefore reasonable to assume, that the chloride anions influencing the step fluctuations are merely the anions adsorbed at step sites in accordance with the $t^{1/4}$-law measured in the anodic potential range. For the Au(111) sample used in our experiments presented here, the mean concentration of step sites was about 5×10^{-3} per atom. If specific adsorption of chloride starts at step sites these adsorption sites, however, are saturated already for small chloride concentrations. When the steps are covered by chloride, adsorption starts on the terraces. Since mass transport is dominated by edge diffusion, the step fluctuations then are not further increased and F(t) becomes independent of the chloride amount on the surface.

A saturation of step sites for small amounts of chloride in the electrolyte is confirmed by the current-potential curve for electrolyte (B) (Fig. 7 (b)). For a chloride concentration of 0.01mM in 0.1M sulfuric acid the formation of an ordered sulfate layer is still observed at + 786mV vs. SCE, however, no satellite peaks occur at slightly more anodic potentials as is typical for the current-potential curves of pure 0.1M sulfuric acid (Fig. 7 (a)). It is reasonable to assume that initially the replacement of sulfate by chloride is kinetically more favorable at step sites compared to terrace sites, and hence, the ordered sulfate layer is still formed on the terraces giving rise to

a peak at +786mV. The vanishing of the satellite peaks for 0.01mM Cl^- in the electrolyte can therefore be attributed to chloride adsorbed at the step edges.

4.3 Quantitative analysis of the potential dependence of F(t)

Finally, we want to analyze our data for the chloride-containing electrolytes (B)-(F) with respect to the energy-related quantities involved in the step fluctuations.

(a) Electrode potentials U_s < + 300mV vs. SCE

First we focus on the results measured for electrode potentials U_s < + 300mV vs. SCE. Here, we find a time law for the time correlation function as given in eq. (6) for all electrolytes. Eq. (6) can be rewritten as

$$F(t) = \sqrt{2\nu_a}\; a_\perp^2\; e^{-\varepsilon/2k_BT}\; e^{-E_{ad}^{\neq}/2k_BT}\; t^{1/2} \qquad (11)$$

where we used $P_k \approx 2\; a_\perp^2/a_\parallel\; \exp(-\varepsilon/k_BT)$ and replaced τ_a by $\nu_a^{-1} \exp\left(E_{ad}^{\neq}/k_BT\right)$, $E_{ad}^{\neq}$ being the activation energy for adatom creation and ν_a being the pre-exponential factor[4]. In contrast to the kink creation, the formation of an terrace adatom is associated with a large dipole moment. Hence, the activation energy for adatom creation $E_{ad}^{\neq}$ should depend on the electrode potential, whereas the kink formation

[4] The activation energy for adatom creation $E_{ad}^{\neq}$ is indeed an activation energy and thus equal or larger than the energy for adatom formation from kinks. The difference in the interpretation of the activation energy for adatom creation becomes obvious from the scaling theory of Pimpinelli et al. [21]. In the case of Au(111) at U_S < + 300mVs. SCE, the dominant mass transport is analog to "Case B" (corresponding to eq.(11) above) of Pimpinelli et al. [21] which contains the adatom creation rate rather than the equilibrium concentration of adatoms on the terrace. Hence, eq.(11) contains a pre-exponential factor ν_a and $E_{ad}^{\neq}$ is an activation energy.

energy ε should be approximately potential independent. To describe this influence on $E_{ad}^{\neq}$, we use a linear ansatz similar to what is discussed in ref. [8][5]:

$$E_{ad}^{\neq} = E_{ad}^{0} - \lambda^{-}\, eU_S \qquad (12)$$

The activation energy E_{ad}^{0} at U_S = 0V vs. SCE merely serves as a reference point to define the linear relation between electrode potential and energy. Likewise, λ^{-} is the factor which describes the linear dependence between the electrode potential and energy and must not be confused with the charge transfer coefficient. Using eqs. (11),(12) one obtains for t=1 s

$$F(1s) = \sqrt{2\nu_a}\, a_{\perp}^{2}\, e^{-\left(\varepsilon + E_{ad}^{0}\right)/2k_BT}\, e^{\lambda^{-} eU_S/2k_BT} \quad \left[s^{1/2}\right] \qquad (13)$$

For Ag(111) in solution, it was shown that F(t) is independent of the potential in the far cathodic potential range. In this potential range, F(t) can be approximated by a constant value which is equal to the value of the time correlation function measured under UHV conditions at room temperature [8]. From Fig. 5 we find that for Au(111) in all electrolytes F(1s) in the negative potential range is independent on the electrode potential and may also be approximated by a constant value. The average

[5] Recently, Haftel and Einstein used the surface-embedded-atom-model [57, 58] to determine the dependence of diffusion barriers on the charge deposited on the metal electrode by the electrical double layer [59]. They show that diffusion barriers may depend substantially - and not necessarily linearly - on the charge. In the case of small variations in the charge (i.e. for small differences in the electrode potential), however, the functional dependence of the activation energies for atomic mass transport can be approximated by a linear function.

value as determined from all our data in the range $U_s < -50\text{mV}$ vs. SCE is $1.6 \pm 0.5\ a_\perp^2$.

We have fitted the experimental data in Fig. 5 for the chloride containing electrolytes (B) and (C)-(F) separately to an exponential of the form[6]

$$\frac{F(1s)}{a_\perp^2} = 1.6 + C_{1/2}\ e^{\frac{\lambda^- eU_s}{2k_BT}} \qquad (14)$$

where the factor $C_{1/2}$ is determined by eq. (13): $C_{1/2} = \sqrt{2\nu_a}\ e^{-\left(\varepsilon + E_{ad}^0\right)/2k_BT}\left[s^{1/2}\right]$.

Fitting eq.(14) to the averaged data for high concentrations (electrolytes (C)-(F), open circles in Fig. 5) and to the data for electrolyte (B) (0.01mM HCl, open squares) we find

$$\sqrt{2\nu_a}\ e^{-\left(\varepsilon + E_{ad}^0\right)/2k_BT}\left[s^{1/2}\right] = \begin{cases} 0.8 \pm 0.3 & (C)-(F) \\ 0.9 \pm 1.1 & (B) \end{cases} \qquad (15)$$

and

$$\lambda^- = \begin{cases} 0.4 \pm 0.1 & (C)-(F) \\ 0.2 \pm 0.3 & (B) \end{cases} \qquad (16)$$

[6] We have also analyzed the data by fitting an exponential without a constant contribution. The results remain basically unchanged. The energies obtained are of the same order of magnitude.

Assuming a typical pre-exponential factor for the adatom creation of $\nu_a \sim 10^{13}\ s^{-1}$ for all electrolytes we obtain

$$\varepsilon + E_{ad}^{0} = \begin{cases} 0.7 \pm 0.1\ eV/atom & (C)-(F) \\ 0.8 \pm 0.1 eV/atom & (B) \end{cases} \qquad (17)$$

The error bars given in eq. (17) represent the statistical error. The energies we obtain can only serve as an estimate, and should not be considered as exact values since systematic errors may introduce larger error bars into eq.(17). The energy $E_{ad}^{\neq}$ at U_S = 0V vs. SCE given in eq. (17) seems to be approximately independent on the chloride concentration, and within the error bars also the value of λ^{-} does not significantly depend on the electrolyte.

For Au(111) in electrolyte (C) (containing 0.5mM HCl) we find for the kink formation energy at U_s = – 100mV vs. SCE ε^{Cl^-} = 0.074 ± 0.002 eV/atom (eq.(10), Fig. 6), which is in agreement with effective medium theory (EMT) calculations for Au(111) in UHV [52]. The agreement, however, may be somewhat accidental since the calculations were performed for the unreconstructed gold surface. A kink energy of ε = 0.074eV should nevertheless be of the right order of magnitude. We assume that the kink formation energy does not depend on the electrode potential. This is a reasonable assumption (at least as the order of magnitude is concerned) because the formation of a kink is associated with a very small dipole moment, and hence, should not be dramatically affected by the electrode potential. For Ag(111) in electrolyte, it was indeed shown experimentally [8, 9, 60] as well as theoretically [59] that the kink energy is potential independent. In addition, we assume that the kink energy does not depend on the amount of chloride in the electrolyte. This

assumption is realistic since chloride initially adsorbs at steps (compare Fig. 5) and blocks the step sites. When the step sites are saturated, chloride adsorbs on the terrace and has presumably no further influence on the kink creation energy. The adatom creation energy on gold at U_S = 0V may then be estimated using eq. (17) to be of the order of

$$E_{ad}^{0} = 0.7 \text{ eV / atom} \qquad (18)$$

nearly independent on the electrolyte. From the $t^{1/2}$-law of F(t) for low potentials we know that terrace diffusion is faster than atom detachment at steps, i.e., the terrace diffusion barrier must be considerably smaller than $E_{ad}^{0} = 0.7 \text{ eV / atom}$. Hence, it is reasonable to assume that the terrace diffusion barrier for Au(111) in electrolyte may be of comparable size as in UHV (~ 0.1eV [52]).

E_{ad}^{0} is the activation energy of the creation of an adatom on the Au(111) terrace at the solid/liquid interface which may be compared with typical values for the adatom creation energy in UHV. Using effective medium calculations, Stoltze [52] determined the adatom formation energy from kink sites. In order to compare his data with our result one has to consider that the energies by Stoltze are adatom *formation* energies rather than *activation* energies for the creation adatoms. To estimate the activation energies in UHV from ref. [52] it is reasonable to assume that the activation energy for adatom creation can be approximated by the sum of the formation energy and the diffusion barrier of Au adatoms on the surface (see Fig. 8). Then, one finds e.g. for the activation energy for adatom creation from kink sites on Au(111) in UHV $E_{ad}+E_{diff}$ ~ 0.67 eV. From experimental data for Cu(111) in UHV e.g. one finds $E_{ad} + E_{diff}$ = 0.76eV/atom [53], which is of the same order of magnitude as

what we find here in the case of Au(111) in electrolyte ($E_{ad}^{0} \sim 0.7$ eV/atom, eq.(18)). The good agreement between the data presented here and calculated and experimental data for metal surfaces in UHV is a surprising result considering that the energetics at the solid/liquid interface may be altered dramatically compared to the solid/vacuum interface.

(b) Electrode potentials U_s > + 300mV vs. SCE

In this potential range, the dominant mass transport is edge diffusion and the time correlation function F(t) is proportional to $t^{1/4}$ (eq. (4)). Inserting $c_{st} = \exp\left(-E_{st}/k_B T\right)$ and $D_{st} = D_0 \exp\left(-E_{diff}/k_B T\right)$ in eq. (4) we obtain

$$F(1s) = \left(8D_0\right)^{1/4} a_{\perp}^{2} \, e^{-\left(3\varepsilon + E_{st} + E_{diff}\right)/4k_B T} \left[s^{1/4}\right] \qquad (19)$$

The diffusion energy E_{diff} is the activation energy for diffusion of atoms along a kinked step, E_{st} is the adatom formation energy from a kink site onto the step edge. Since adatoms at steps and, in particular, adatoms on terraces may be associated with a charge distribution dipole we assume E_{diff} and E_{st} to depend on the electrode potential. The kink formation energy, on the other hand, is assumed to be potential independent as before. Similar to the discussion above we make a linear ansatz for the potential dependence of the energies E_{diff} and E_{st} :

$$\begin{aligned} E_{diff} &= E_{diff}^{0} - \lambda_1^{+} e U_s \\ E_{st} &= E_{st}^{0} - \lambda_2^{+} e U_s \end{aligned} \qquad (20)$$

where λ_1^+, λ_2^+ are the factors to describe the linear relation between energy and electrode potential.

Inserting eq. (20) into eq.(19) yields (with $\lambda^+ = \lambda_1^+ + \lambda_2^+$):

$$F(1s) = (8D_0)^{1/4} a_\perp^2 e^{-\left(3\varepsilon + E_{st}^0 + E_{diff}^0\right)/4k_BT} e^{\lambda^+ eU_s/4k_BT} \left[s^{1/4}\right] \qquad (21)$$

Fitting

$$\frac{F(1s)}{a_\perp^2} = 1.6 + C_{1/4}\, e^{\frac{\lambda^+ eU_S}{4k_BT}} \qquad (22)$$

to the averaged data (electrolytes (C)-(F), open circles in Fig. 5) and to the data for electrolyte (B) (with 0.01mM HCl, open squares) for U_s > + 300mV vs. SCE ($C_{1/4} = (8D_0)^{1/4} e^{-\left(3\varepsilon + E_{st}^0 + E_{diff}^0\right)/4k_BT} \left[s^{1/4}\right]$) we find

$$(8D_0)^{1/4} e^{-\left(3\varepsilon + E_{st}^0 + E_{diff}^0\right)/4k_BT} \left[s^{1/4}\right] = \begin{cases} 1.1 \pm 0.4 & (C)-(F) \\ 0.1 \pm 0.1 & (B) \end{cases} \qquad (23)$$

Further we obtain

$$\lambda^+ = \begin{cases} 0.6 \pm 0.1 & (C)-(F) \\ 0.6 \pm 0.1 & (B) \end{cases} \qquad (24)$$

Using $D_0 \sim 10^{13}\ s^{-1}$ it follows from eq. (23):

$$3\varepsilon + E^0_{st} + E^0_{diff} = \begin{cases} 0.8 \pm 0.1\ \text{eV / atom}\ \ (C)-(F) \\ 0.9 \pm 0.1\ \text{eV / atom}\ \ (B) \end{cases} \qquad (25)$$

Similar to what is found for electrode potentials smaller than + 300mV vs. SCE the sum of the energies in eq. (25) seems to be almost independent on the chloride concentration.

In ref. [52], the diffusion barrier along a straight step on Au(111) in UHV is calculated to E_d = 0.31eV. Based on a work of Natori and Godby [61] who described the diffusion of atoms on a stepped surface we found for the analog one-dimensional case of diffusion along a kinked step [14] that the diffusion barrier E_{diff} along a kinked step may be expressed as $E_{diff} = E_d + \varepsilon$. This equation holds, if the kink formation energy is larger than the activation energy for adatom hopping across a kink site. Using ε^{Cl^-} = 0.074eV for the kink formation energy and E_d = 0.31eV in eq.(25) one obtains for the adatom formation energy $E^0_{st} \sim$ 0.2-0.3eV.

We note that E^0_{st} is the formation energy of a free adsorbed particle at a step where this particle belongs to the mass transport mediating species. For a single system like metal surfaces in UHV or metal electrodes with no specifically adsorbing anions, these particles are adatoms at steps. In the case of Au(111) in chloride containing electrolytes at high potentials, these particles can be of completely different nature. It is not yet clear whether Au adatoms, specifically adsorbed Cl^- at steps or Au-Cl complexes serve as mass transport species. Therefore, we have not yet enough

information to give the formation energy E_{st}^{0} a well defined physical interpretation. The most probable scenario, however, is that Au adatoms and kink atoms diffuse along the steps and cause the steps to appear frizzy in the STM images. In that case, E_{st}^{0} would be the formation energy of Au adatoms at the steps.

5. Conclusions

We have presented a quantitative, detailed study of the dynamics of equilibrium step fluctuations on Au(111) electrodes in chloride-containing and chloride-free electrolytes. From the analysis of the time dependence of the fluctuations we find for the chloride containing electrolytes that far below + 300mV vs. SCE, where the Au (111) surface is reconstructed, the dominant mass transport is fast terrace diffusion and slow attachment/detachment at steps. At electrode potentials larger than + 300mV, the Au(111) surface is unreconstructed and the dominant mass transport is step edge diffusion. A quantitative analysis of the potential dependence of the step fluctuations yielded values of $E_{ad}^{0} = 0.7\ \text{eV}$ for the activation energy for adatom creation on the terraces at U_S = 0V vs. SCE. Since terrace diffusion is fast compared to atom attachment/detachment at steps for small electrode potentials, we conclude that the terrace diffusion barrier is considerably smaller than $E_{ad}^{0} = 0.7\ \text{eV}$ and most probably of the same order as in UHV where one finds E_{diff}~0.1eV. Furthermore, we find $E_{st} \sim 0.2\text{-}0.3$ eV for adatom creation at steps and the kink formation energy in 0.1M H_2SO_4 + 0.5mM HCl $\varepsilon^{Cl} = 0.074\text{eV}$.

Our results show that specifically adsorbed chloride changes the dominant mass transport from terrace diffusion to edge diffusion. This is a surprising result at first glance because it is often believed that the presence of chloride in the electrolyte would favor terrace diffusion against edge diffusion. This understanding is based on

the observation that the ripening of islands on gold surfaces after lifting of the surface reconstruction (which involves terrace diffusion) is faster if chloride is added to the electrolyte. As a caveat we emphasize that this conclusion is not justified: The ripening of islands is a non-equilibrium process where the chemical potential on the surface is not constant. In this case, mass transport processes may occur which are not dominant in the case of equilibrium step fluctuations where the chemical potential on the surface is constant.

A further, unexpected result is that the influence of chloride on the step mobility saturates already for small chloride concentrations and does not further increase even if the chloride amount is increased by several orders of magnitude. We therefore conclude that chloride adsorption starts at steps and adsorption on the terraces has no further influence on the equilibrium step fluctuations which are then dominated by edge diffusion. We, however, emphasize once more that the kinetics of island ripening may still depend on the chloride amount.

In order to fully understand the island ripening on metal electrodes, studies similar to those known from UHV experiments [53, 62-70] (for a review see, e.g., [60]) have to be performed.

Acknowledgment

One of the authors (M. G.) appreciates the hospitality of the Abteilung Elektrochemie, Universität Ulm during her four months stay as a guest researcher with Prof. Dr. D. M. Kolb. In particular, she is indebted to M. Kleinert and L. A. Kibler for their steady support. Financial support was provided by the Fond der Chemischen Industrie, Germany.

References:

[1] J. Canullo, Y. Uchida, G. Lehmpfuhl, T. Twomey, D. M. Kolb, Surf. Sci. 188 (1987) 350.

[2] J. Wiechers, T. Twomey, D. M. Kolb, R. J. Behm, J. Electroanal. Chem. 248 (1988) 451.

[3] G. Binnig, H. Rohrer, C. Gerber, Appl. Phys. Lett. 40 (1982) 178.

[4] D. M. Kolb, Prog. Surf. Sci. 51 (1996) 109.

[5] M. Dietterle, T. Will, D. M. Kolb, Surf. Sci. 327 (1995) L495.

[6] O. M. Magnussen, M. R. Vogt, J. Scherer, R. J. Behm, Appl. Phys. A 66 (1998) 447.

[7] M. Wilms, P. Broekmann, M. Kruft, C. Stuhlmann, K. Wandelt, Appl. Phys. A 66 (1998) 473.

[8] M. Giesen, M. Dietterle, D. Stapel, H. Ibach, D. M. Kolb, Surf. Sci. 384 (1997) 168.

[9] M. Giesen, R. Randler, S. Baier, H. Ibach, D. M. Kolb, Electrochim. Acta 45 (1999) 533.

[10] S. Baier, M. Giesen, Phys. Chem. Chem. Phys. 2 (2000) 3675.

[11] M. Giesen-Seibert, R. Jentjens, M. Poensgen, H. Ibach, Phys. Rev. Lett. 71 (1993) 3521.

[12] M. Giesen-Seibert, R. Jentjens, M. Poensgen, H. Ibach, Phys. Rev. Lett. 73 (1994) E911.

[13] M. Giesen, G. S. Icking-Konert, Surf. Sci. 412/413 (1998) 645.

[14] M. Giesen, G. S. Icking-Konert, D. Stapel, H. Ibach, Surf. Sci. 366 (1996) 229.

[15] L. Kuipers, M. S. Hoogeman, J. W. M. Frenken, Phys. Rev. Lett. 71 (1993) 3517.

[16] L. Masson, L. Barbier, J. Cousty, Surf. Sci. 317 (1994) L1115.

[17] L. Masson, L. Barbier, J. Cousty, B. Salanon, Surf. Sci. 324 (1994) L378.

[18] S. Speller, W. Heiland, A. Biedermann, E. Platzgummer, C. Nagl, M. Schmid, P. Varga, Surf. Sci. 331-333 (1995) 1056.

[19] N. C. Bartelt, J. L. Goldberg, T. L. Einstein, E. D. Williams, J. C. Heyraud, J. J. Métois, Phys. Rev. B48 (1993) 15453.

[20] N. C. Bartelt, T. L. Einstein, E. D. Williams, Surf. Sci. 312 (1994) 411.

[21] A. Pimpinelli, J. Villain, D. E. Wolf, J. J. Métois, J. C. Heyraud, I. Elkinani, G. Uimin, Surf. Sci. 295 (1993) 143.

[22] S. V. Khare, T. L. Einstein, Phys. Rev. B 57 (1998) 4782.

[23] B. Blagojevic, P. M. Duxbury, Phys. Rev. B 60 (1999) 1279.

[24] C. E. Bach, R. J. Nichols, W. Beckmann, H. Meyer, A. Schulte, J. O. Besenhard, P. D. Jannakoudakis, J. Electrochem. Soc. 140 (1993) 2181.

[25] L. A. Nagahara, T. Thundat, P. I. Oden, S. M. Lindsay, Ultramicroscopy 33 (1990) 107.

[26] D. M. Kolb, in J. Lipkowsky, P. N. Ross (Eds.): *Structure of Electrified Interfaces*, VCH, New York 1993, p. 65.

[27] N. Kitamura, M. G. Lagally, M. B. Webb, Phys. Rev. Lett. 71 (1993) 2082.

[28] J. F. Wolf, B. Vicenzi, H. Ibach, Surf. Sci. 249 (1991) 233.

[29] M. Poensgen, J. F. Wolf, J. Frohn, M. Giesen, H. Ibach, Surf. Sci. 274 (1992) 430.

[30] M. Giesen-Seibert, H. Ibach, Surf. Sci. 316 (1994) 205.

[31] J. Li, R. Berndt, W.-D. Schneider, Phys. Rev. Lett. 76 (1996) 1888.

[32] P. Broekmann, M. Wilms, M. Kruft, C. Stuhlmann, K. Wandelt, J. Electroanal. Chem. 467 (1999) 307.

[33] M. R. Vogt, A. Lachenwitzer, O. M. Magnussen, R. J. Behm, Surf. Sci. 399 (1998) 49.

[34] R. McHardy, W. H. Haiss, R. J. Nichols, Phys. Chem. Chem. Phys. 2 (2000) 1439.

[35] N. C. Bartelt, J. L. Goldberg, T. L. Einstein, E. D. Williams, Surf. Sci. 273 (1992) 252.

[36] N. C. Bartelt, T. L. Einstein, E. D. Williams, Surf. Sci. 240 (1990) L591.

[37] G. Ehrlich, F. G. Hudda, J. Chem. Phys. 44 (1966) 1039.

[38] R. L. Schwoebel, E. J. Shipsey, J. Appl. Phys. 37 (1966) 3682.

[39] J. L. Stickney, I. Villegas, C. B. Ehlers, J. Am. Chem. Soc. 111 (1989) 6473.

[40] A. S. Dakkouri, Solid State Ionics 94 (1997) 99.

[41] D. M. Kolb, J. Schneider, Electrochim. Acta 31 (1986) 929.

[42] U. W. Hamm, D. Kramer, R. S. Zhai, D. M. Kolb, J. Electroanal. Chem. 414 (1996) 85.

[43] A. Hamelin, T. Vitanov, E. Sevastyanov, A. Popov, J. Electroanal. Chem. 145 (1983) 225.

[44] Z. Shi, S. Wu, J. Lipkowski, Electrochim. Acta 40 (1995) 9.

[45] O. M. Magnussen, J. Hageböck, J. Hotlos, R. J. Behm, Faraday Discuss. Chem. Soc. 94 (1992) 329.

[46] M. Giesen-Seibert, F. Schmitz, R. Jentjens, H. Ibach, Surf. Sci. 329 (1995) 47.

[47] G. J. Edens, X. Gao, M. J. Weaver, J. Electroanal. Chem. 375 (1994) 357.

[48] M. Ito, private communication (1996) .

[49] B. M. Ocko, O. M. Magnussen, J. X. Wang, R. R. Adzic, T. Wandlowski, Physica B 221 (1996) 238.

[50] L. A. Kibler, D. M. Kolb, unpublished (1999) .

[51] D. A. Scherson, D. M. Kolb, J. Electroanal. Chem. 176 (1984) 353.

[52] P. Stoltze, J. Phys. Condens. Matter 6 (1994) 9495.

[53] G. S. Icking-Konert, M. Giesen, H. Ibach, Surf. Sci. 398 (1998) 37.

[54] Z. Shi, J. Lipkowski, J. Electroanal. Chem. 403 (1996) 225.

[55] J. A. Meyer, P. Schmid, R. J. Behm, Phys. Rev. Lett. 74 (1995) 3864.

[56] C. Ratsch, A. P. Seitsonen, M. Scheffler, Phys. Rev. B55 (1997) 6750.

[57] M. I. Haftel, Phys. Rev. B48 (1993) 2611.

[58] M. I. Haftel, M. Rosen, S. G. Corcoran, in P. C. Andricacos, S. G. Corcoran, J.-L. Delplancke, T. P. Moffat, P. C. Searson (Eds.): *Electrochemical Synthesis and Modification of Materials, Vol. 451*, MRS, Pittsburgh 1997, p. 31.

[59] M. I. Haftel, T. L. Einstein, in A. Gonis, P. E. A. Turchi, A. J. Ardell (Eds.): *Nucleation and Growth Processes in Materials, Vol. 580*, MRS, Pittsburgh 2000, p. in press.

[60] M. Giesen, Prog. Surf. Sci. 65 (2000), in press.

[61] A. Natori, R. W. Godby, Phys. Rev. B47 (1993) 15816.

[62] W. Theis, N. C. Bartelt, R. M. Tromp, Phys. Rev. Lett. 75 (1995) 3328.

[63] J. B. Hannon, C. Klünker, M. Giesen, H. Ibach, N. C. Bartelt, J. C. Hamilton, Phys. Rev. Lett. 79 (1997) 2506.

[64] C. Klünker, J. B. Hannon, M. Giesen, H. Ibach, G. Boisvert, L. J. Lewis, Phys. Rev. B 58 (1998) R7556.

[65] K. Morgenstern, G. Rosenfeld, B. Poelsema, G. Comsa, Phys. Rev. Lett. 74 (1995) 2058.

[66] K. Morgenstern, G. Rosenfeld, G. Comsa, Phys. Rev. Lett. 76 (1996) 2113.

[67] K. Morgenstern, G. Rosenfeld, E. Laegsgaard, F. Besenbacher, G. Comsa, Phys. Rev. Lett. 80 (1998) 556.

[68] G. Rosenfeld, K. Morgenstern, M. Esser, G. Comsa, Appl. Phys. A69 (1999) 489.

[69] G. Rosenfeld, K. Morgenstern, I. Beckmann, W. Wulfhekel, E. Laegsgaard, F. Besenbacher, G. Comsa, Surf. Sci. 402-404 (1998) 401.

[70] M. Giesen, G. S. Icking-Konert, H. Ibach, Surf. Sci. 431 (1999) 109.

Figure Captions:

Fig. 1: Time images of steps on Au (111) in 0.1M H_2SO_4 + 5 mM HCl at (a) 0 mV and (b) +400mV vs. SCE. The scan width is 150 nm in both images. The slight shift of the step edge position to the left with increasing time (top to bottom of the image) is due to thermal drift which is accounted for in our analysis by making use of eq. (2).

Fig. 2: Time correlation function F(t) (eq. (2)) as measured for Au(111) at (a) + 200 mV and (b) + 600mV vs. SCE in 0.1M H_2SO_4 + 1mM HCl. The solid and dashed curves are fits to a power law t^{α} with α = 1/2 and 1/4. For electrode potentials U_s < +300mV vs. SCE, F(t) is well fitted by a time exponent 1/2, while for U_s > +300mV vs. SCE better agreement is achieved for a time exponent 1/4.

Fig. 3: Time correlation function F(t) measured as a function of the step-step distance L for (a) U_s = + 250mV and (b) U_s = + 600mV vs. SCE. The circles are the experimental data. The solid lines represent best fits to the data assuming that the step fluctuations are independent of L, i.e. δ = 0 (eq. (3)). The dashed lines are fits to exponents (a) δ=0.25 and (b) $\delta=\pm 0.5$ (see text for discussion).

Fig. 4: F(1s) vs. the electrode potential for different chloride concentrations as shown in the figure. The solid and dotted lines are fits to exponential functions (see text for discussion).

Fig. 5: Plot of F(1s) for Cl^- concentrations larger than 0.01mM (circles), equal to 0.01mM (open squares) and for Cl^--free H_2SO_4 (triangles). The lines are fits to exponentials as discussed in the text.

Fig. 6:

Spatial correlation function F(y) measured for Au(111) in 0.1M H_2SO_4 + 0.5mM HCl at U_S = −100mV vs. SCE.

Fig. 7: Cyclic voltammograms for Au(111) in (a) 0.1M H_2SO_4, (b) 0.1M H_2SO_4 + 0.01mM HCl and (c) 0.1M H_2SO_4 + 1mM HCl. Scan rate: 10mV/s.

Fig. 8: Potential diagram of the energies related to the detachment of atoms from steps onto the terrace. The activation energy E_{ad}^{0} for adatom creation may be approximated by the sum of the adatom formation energy E_{ad} and the terrace diffusion barrier E_{diff}.

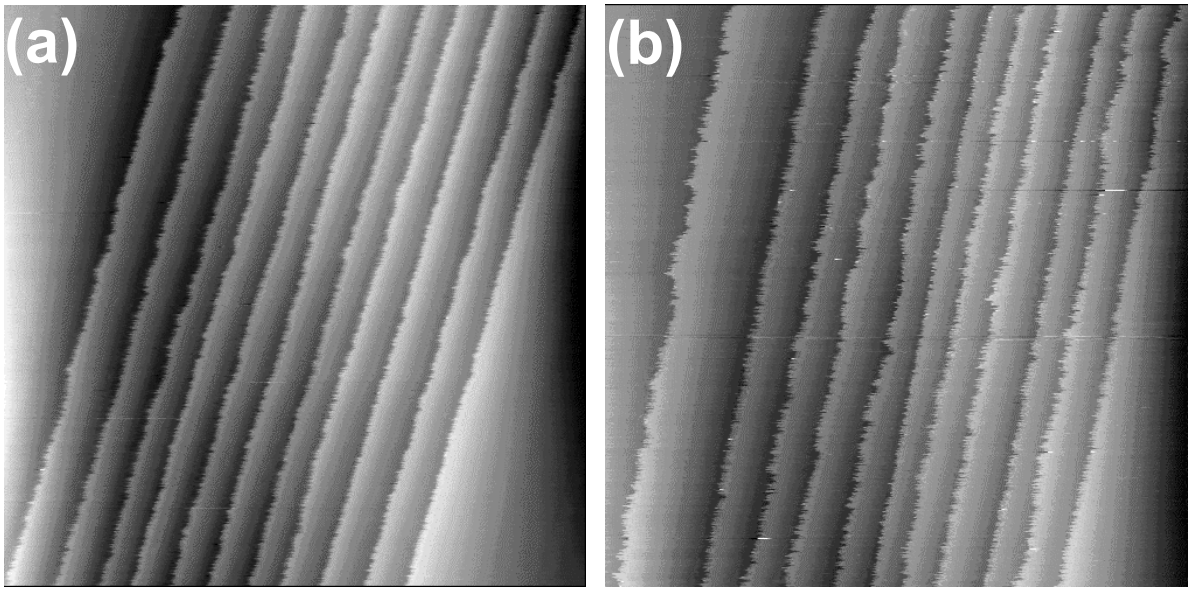

Fig. 1

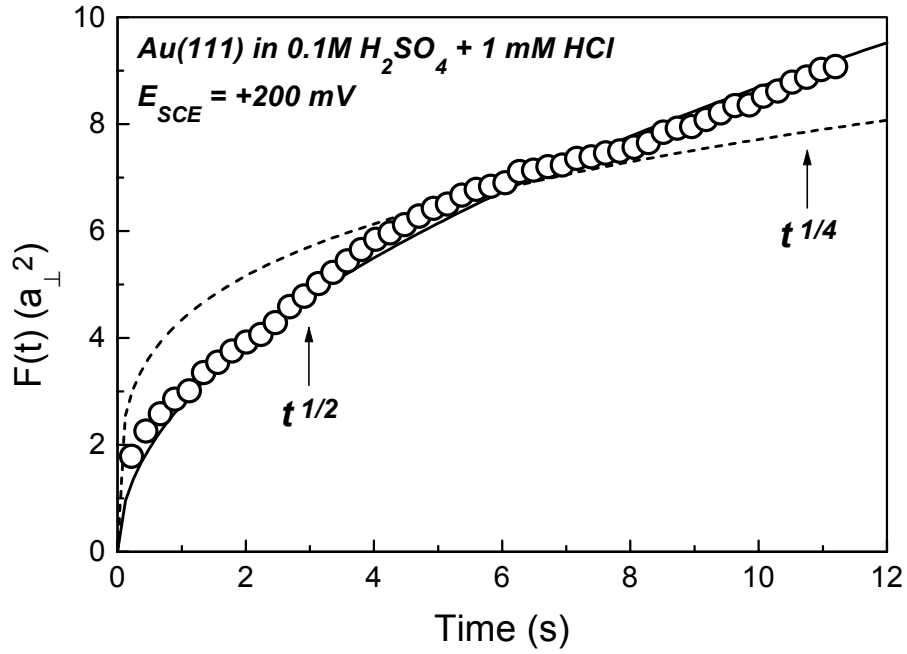
Au(111) in 0.1M H2SO4 + 1 mM HCl
ESCE = +200 mV
t 1/4
t 1/2
F(t) (a⊥2)
Time (s)
0
2
4
6
8
10
12

Fig. 2(a)

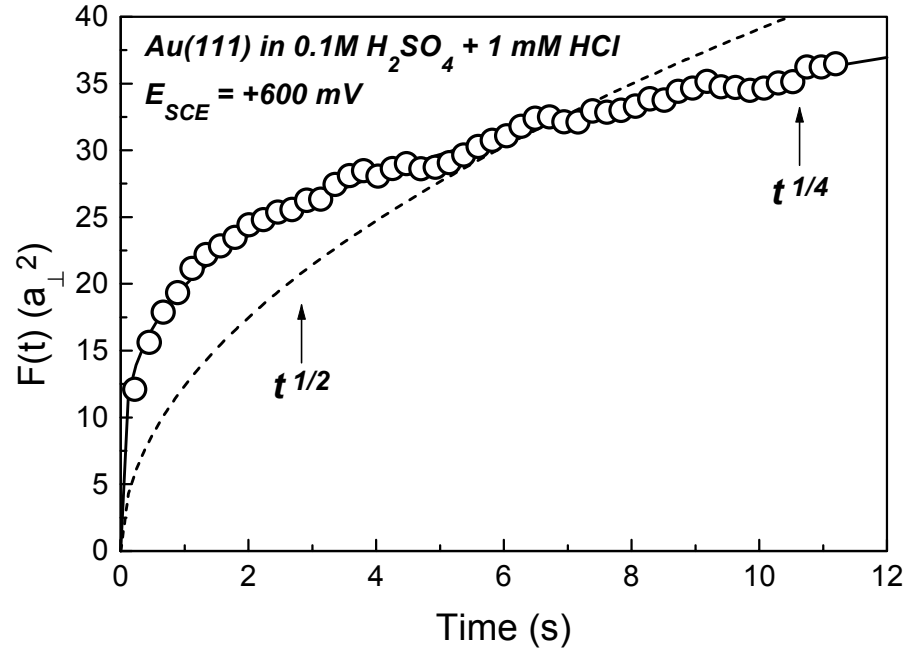
Au(111) in 0.1M H2SO4 + 1 mM HCl
ESCE = +600 mV
t 1/4
t 1/2
F(t) (a⊥2)
Time (s)
0
5
10
15
20
25
30
35
40
0
2
4
6
8
10
12

Fig. 2(b)

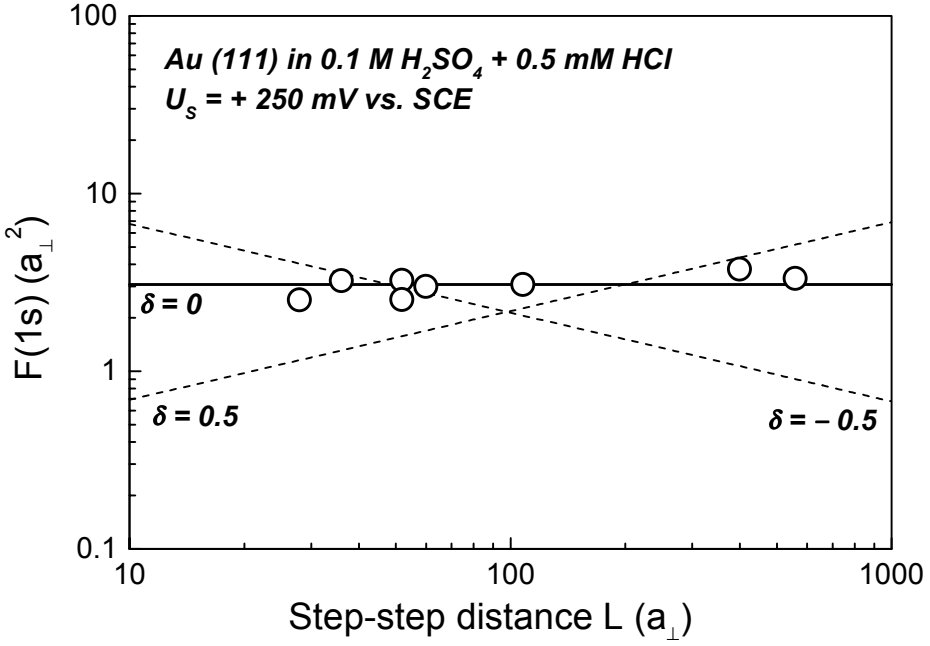
Au (111) in 0.1 M H2SO4 + 0.5 mM HCl
Us = + 250 mV vs. SCE
δ = 0
δ = 0.5
δ = – 0.5
F(1s) (a⊥2)
Step-step distance L (a⊥)
100
10
1
0.1
10
100
1000

Fig. 3(a)

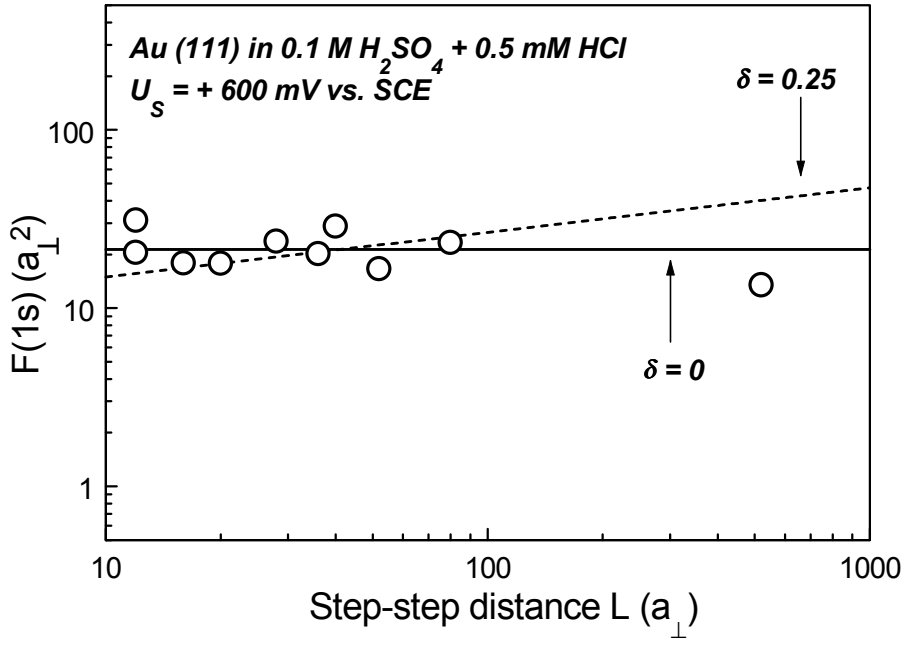
Au (111) in 0.1 M H2SO4 + 0.5 mM HCl
Us = + 600 mV vs. SCE
δ = 0.25
δ = 0
F(1s) (a⊥2)
Step-step distance L (a⊥)
100
10
1
10
100
1000

Fig. 3(b)

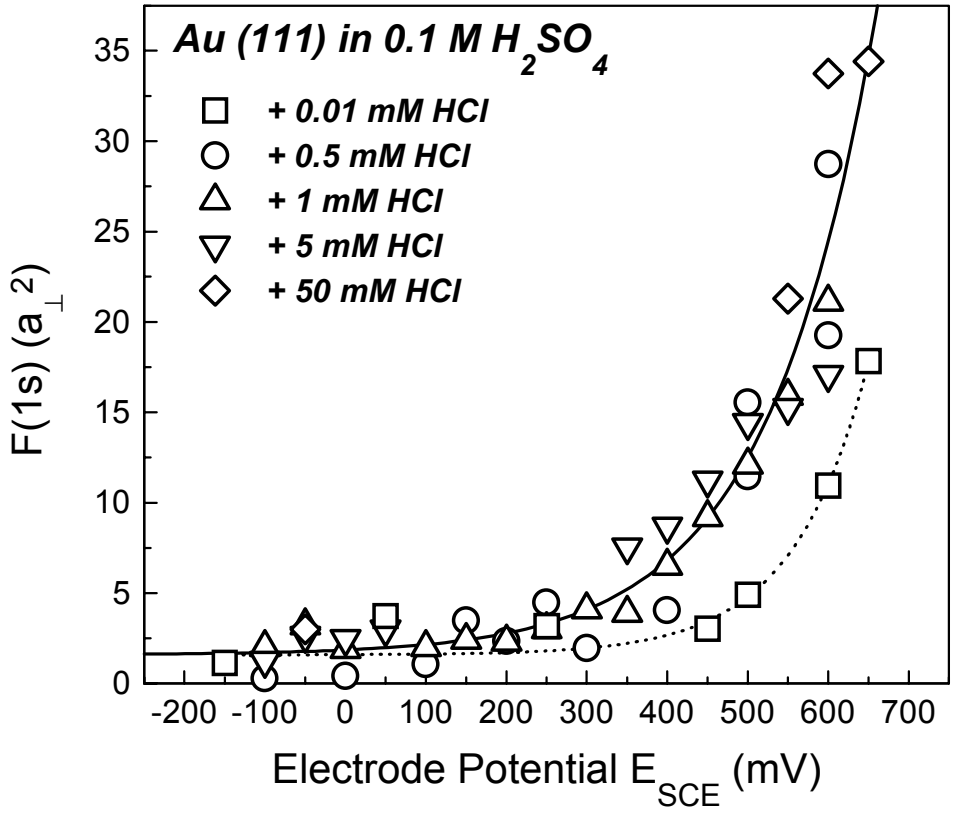
Au (111) in 0.1 M H2SO4
+ 0.01 mM HCl
+ 0.5 mM HCl
+ 1 mM HCl
+ 5 mM HCl
+ 50 mM HCl
F(1s) (a⊥2)
Electrode Potential ESCE (mV)
0
5
10
15
20
25
30
35
-200
-100
0
100
200
300
400
500
600
700

Fig. 4

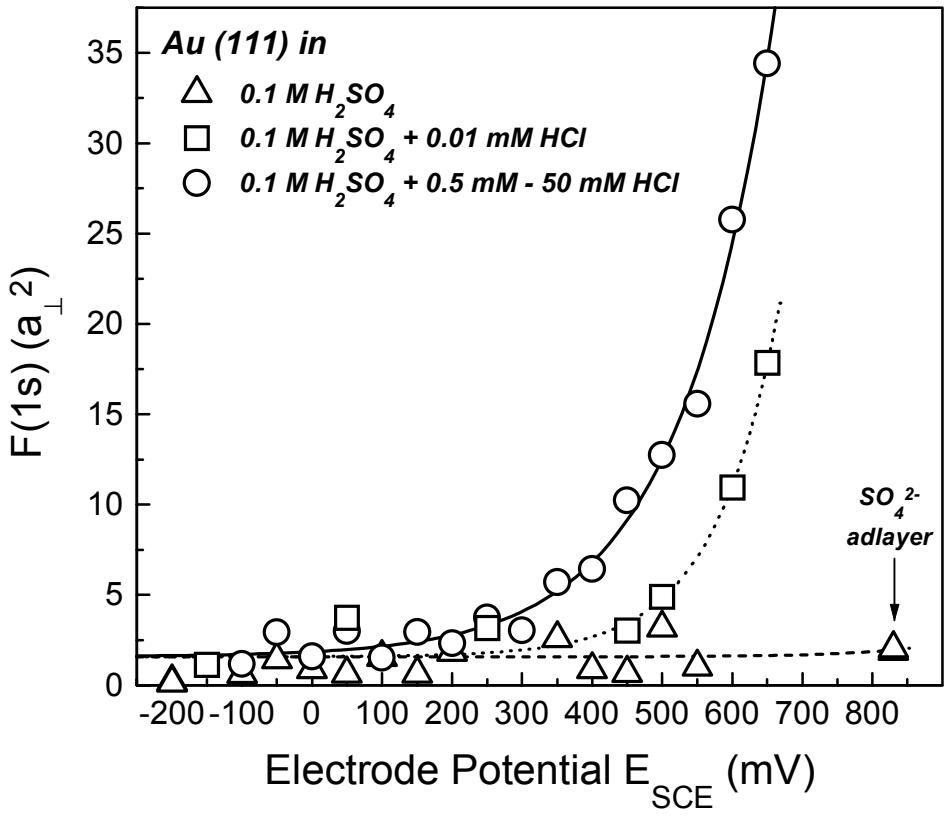
Au (111) in
0.1 M H2SO4
0.1 M H2SO4 + 0.01 mM HCl
0.1 M H2SO4 + 0.5 mM - 50 mM HCl
SO4 2- adlayer
F(1s) (a⊥2)
Electrode Potential ESCE (mV)
0
5
10
15
20
25
30
35
-200 -100 0 100 200 300 400 500 600 700 800

Fig. 5

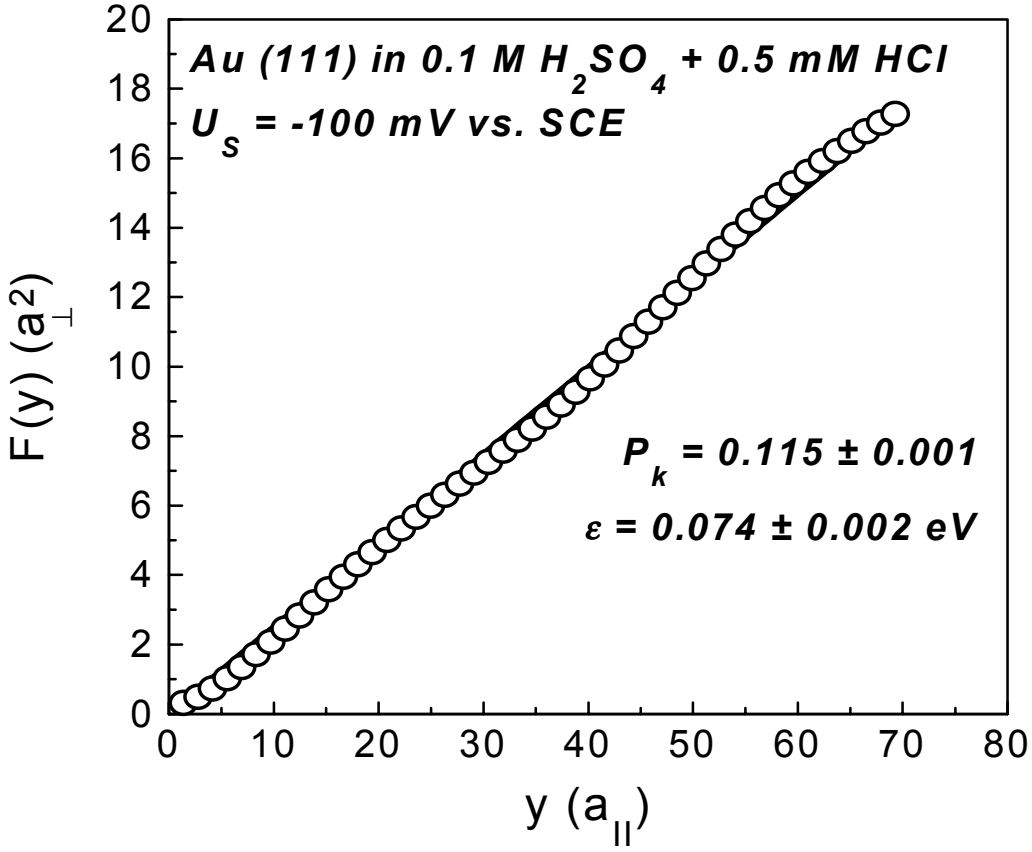
Au (111) in 0.1 M H2SO4 + 0.5 mM HCl
US = -100 mV vs. SCE
Pk = 0.115 ± 0.001
ε = 0.074 ± 0.002 eV
F(y) (a⊥2)
y (a||)
0
2
4
6
8
10
12
14
16
18
20
0
10
20
30
40
50
60
70
80

Fig. 6

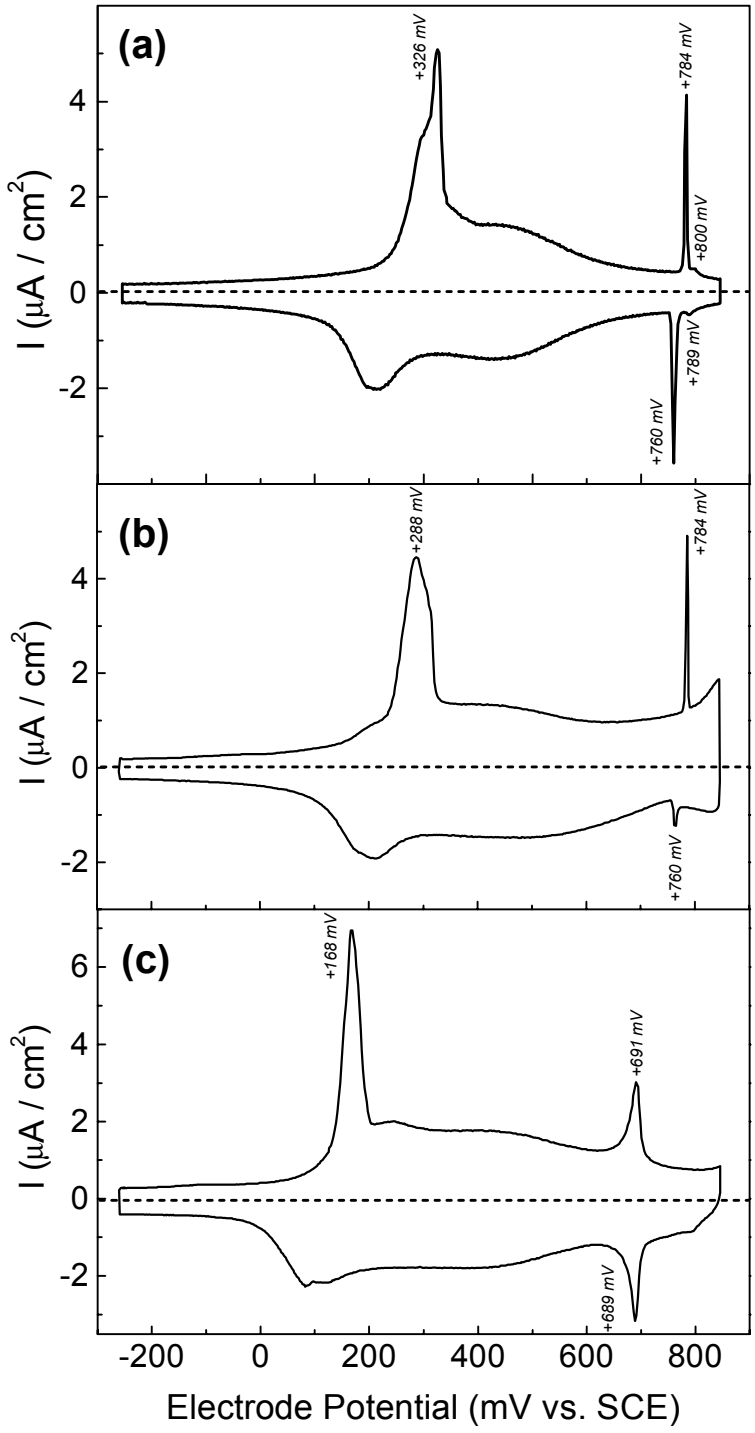
(a)
+326 mV
+784 mV
+800 mV
+789 mV
+760 mV
(b)
+288 mV
+784 mV
+760 mV
(c)
+168 mV
+691 mV
+689 mV
I (μA / cm²)
Electrode Potential (mV vs. SCE)

Fig. 7

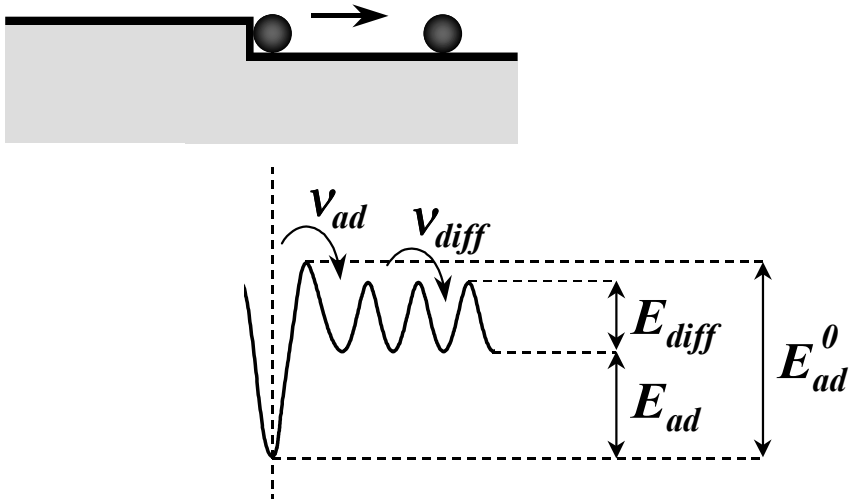

Fig. 8